HHS Public Access

Author manuscript

Chem Mater. Author manuscript; available in PMC 2017 August 23.

Published in final edited form as:

Chem Mater. 2016 August 23; 28(16): 5962–5972. doi:10.1021/acs.chemmater.6b02634.

Understanding Acoustic Cavitation Initiation by Porous Nanoparticles: Toward Nanoscale Agents for Ultrasound Imaging and Therapy

Adem Yildirim[†,*], **Rajarshi Chattaraj**[‡,#], **Nicholas T. Blum**[†,#], and **Andrew P. Goodwin**[†,*]

[†]Department of Chemical and Biological Engineering, University of Colorado Boulder. Boulder, Colorado 80303, United States

[‡]Department of Mechanical Engineering, University of Colorado Boulder. Boulder, Colorado 80309, United States

Abstract

Ultrasound is widely applied in medical diagnosis and therapy due to its safety, high penetration depth, and low cost. In order to improve the contrast of sonographs and efficiency of the ultrasound therapy, echogenic gas bodies or droplets (with diameters from 200 nm to 10 μm) are often used, which are not very stable in the bloodstream and unable to penetrate into target tissues. Recently, it was demonstrated that nanobubbles stabilized by nanoparticles can nucleate ultrasound responsive microbubbles under reduced acoustic pressures, which is very promising for the development of nanoscale (<100 nm) ultrasound agents. However, there is still very little understanding about the effects of nanoparticle properties on the stabilization of nanobubbles and nucleation of acoustic cavitation by these nanobubbles. Here, a series of mesoporous silica nanoparticles with sizes around 100 nm but with different morphologies were synthesized to understand the effects of nanoparticle porosity, surface roughness, hydrophobicity, and hydrophilic surface modification on acoustic cavitation inception by porous nanoparticles. The chemical analyses of the nanoparticles showed that, while the nanoparticles were prepared using the same silica precursor (TEOS) and surfactant (CTAB), they revealed varying amounts of carbon impurities, hydroxyl content, and degrees of silica crosslinking. Carbon impurities or hydrophobic modification with methyl groups is found to be essential for nanobubble stabilization by mesoporous silica nanoparticles. The acoustic cavitation experiments in the presence of ethanol and/or bovine serum albumin (BSA) demonstrated that acoustic cavitation is predominantly nucleated by the nanobubbles stabilized at the nanoparticle surface not inside the mesopores. Finally, acoustic cavitation experiments with rough and smooth nanoparticles were suggested that a rough nanoparticle surface is needed to largely preserve surface nanobubbles after coating the surface with hydrophilic macromolecules, which is required for in vivo applications of nanoparticles.

[*]**Corresponding Author**. (Andrew P. Goodwin): andrew.goodwin@colorado.edu, (Adem Yildirim): adem.yildirim@colorado.edu.
[#]Rajarshi Chattaraj and Nicholas T. Blum contributed equally to this manuscript.

Supporting Information

A PDF containing additional figures and a table. This material is available free of charge via the Internet at http://pubs.acs.org.

Author Contributions

The manuscript was written through contributions of all authors. All authors have given approval to the final version of the manuscript.

Graphical Abstract

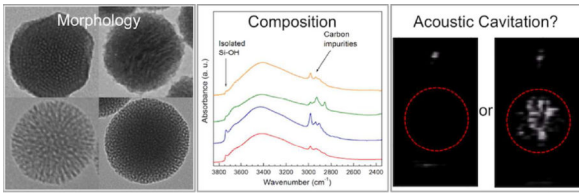

INTRODUCTION

Owing to its safety, substantial tissue penetration depth, and low cost, ultrasound has been utilized extensively for various biomedical applications such as diagnostic medical sonography, ablation of solid tumors, treatment of Alzheimer's disease, and improved drug delivery by sonoporation.[1–8] Ultrasound contrast agents such as micron-scale fluorocarbon bubbles and submicron fluorocarbon droplets greatly improve image contrast and spatial resolution.[9–19] In addition, ultrasound agents have been demonstrated to improve drug perfusion and gene delivery via localized cavitation agents and resultant sonoporation.[20–26] However, current ultrasound agents are too large and unstable in the bloodstream to effectively accumulate and penetrate into the target tissues. For instance, by considering vascular, transvascular, and interstitial transport of the particles in the tumors, the particles should be smaller than 200 nm (preferably in the size range of 12–50 nm) for deep tumor penetration,[2, 27] while bubbles and droplets for ultrasound imaging have typical diameters in the ranges of 1–10 μm and 200 nm−1 μm, respectively.[9, 23]

A promising way to overcome these limitations is to instead administer nanoparticles that can stabilize nanobubbles on their surface and/or inside the well-defined cavities.[28–34] These nanobubbles can initiate acoustic inertial cavitation, which is the process of spontaneous growth of water bubbles followed by violent collapse. The nanobubbles remain stable on the particle surface but grow when exposed to sufficient negative acoustic pressures by externally applied ultrasound.[35–38] Recently, we and others showed that acoustic cavitation can be induced at clinically relevant acoustic pressures via the interaction of sound with hydrophobic mesoporous silica nanoparticles,[28, 29] polystyrene nanocups,[30, 33] and solid polytetrafluoroethylene (PTFE) nanoparticles.[31] These generated bubbles can not only be imaged using conventional ultrasound,[29] but the shock waves emitted by the acoustic cavitation process can kill cancer cells[28, 32] and facilitate drug delivery in vivo.[33] Thus, while it is generally known that nanobubbles are stabilized by hydrophobic interfaces,[39–42] there is still little understanding about the relationship between nanoparticle properties and the efficiency of acoustic cavitation. In this paper, we show the effect of such parameters as nanoparticle porosity, chemical modification, and surface roughness on nanobubble stabilization and acoustic cavitation by mesoporous silica nanoparticles. From these studies, we elucidate the role of particle morphology and surface chemistry on the stabilization of nanobubbles to help design efficient nanoscale ultrasound agents for future in vivo studies and clinical trials.

RESULTS

To study the effects of porosity, pore structure, and surface morphology on acoustic cavitation by porous nanoparticles, different types of silica nanoparticles were prepared with similar particle sizes and synthetic pathways but different final morphologies. Each nanoparticle formulation was prepared using tetraethylorthosilicate (TEOS) as silica source and cetyl trimethylammonium bromide (CTAB) as a structure directing agent but at different experimental conditions (see the Experimental Section for details). First, MCM-41 type mesoporous silica nanoparticles (MSN) were synthesized with a hexagonally ordered pore structure, which we had shown in previous studies acted as a vapor-nucleating nanoparticle if modified with hydrophobic octyl chains.[29] Next, two MCM-48 type MSNs were prepared with cubic pore structures, and smooth and rough surfaces, respectively. As a different pore morphology, a MSN was formulated at neutral conditions with non-organized pore structure, as well as a MSN with dendritic pore structure by slightly modifying previous reports.[43–46] Finally, solid silica nanoparticles were prepared using TEOS as silica source according to the Stöber method.[47] These nanoparticles are named MCM-41, MCM-48S, MCM-48R, Random, Dendritic, and Solid, respectively. Purification and surfactant extraction steps were kept the same for each of the nanoparticles; ethanol was used for purification of the particles and surfactant molecules were extracted by refluxing in ethanolic ammonium nitrate solution. All particles were dried overnight at 65 °C and dried powders were stored at RT.

To characterize the particles, Transmission Electron Microscopy (TEM) and Nanoparticle Tracking Analyses (NTA) were performed (Figure 1, Figure S1). According to TEM, all of the particles were around 100 nm in diameter and fairly spherical in shape. However, surface roughness was affected by the different synthesis conditions; for example, the smooth and rough surfaces of MCM-48S and MCM-48R are clearly observed from the insets in Figure 1b and c, respectively. NTA of the particles showed that particles generally had good dispersibility in water, although slight aggregation was observed for MCM-41 and MCM-48 type of MSNs. Particle sizes determined by TEM and NTA and particle numbers in 1 mg mL^{-1} dispersions determined by NTA are summarized in Table 1. Note that although the nanoparticles have similar primary particle sizes, particle numbers of the nanoparticles were in a relatively broad range (0.32×10^{12} – 1.89×10^{12} particles mL^{-1}) since each nanoparticle has different porosity and aggregation number in water.

Next, the ability of each of these nanoparticles to stabilize nanobubbles was determined by measurement of cavitation efficiency by ultrasound imaging. According to the Laplace pressure equation, the internal pressure of a gas bubble (P_i) in water is given as $2\sigma/R$ (by neglecting the ambient pressure), where σ is the surface tension of water and R is the radius of curvature of the interface.[39] The R is always positive for a free bubble, which makes the internal pressure very high especially for small bubbles, and the bubble shrinks with the diffusion of the gas out of the bubble. A bubble trapped in a pore or a surface crack, however, may possess very large or even negative R values, depending on the shape and hydrophobicity of the cavity,[39] which makes the trapped bubble much more stable, as shown through experimental validation.[40, 41] Also, a recent theoretical study showed that nanobubbles which are partially covered with hydrophobic materials can be very stable.[48] Similarly, when dispersed in water the nanoparticles prepared in this work can stabilize

nanobubbles inside their pores and/or surface pits and grooves, which then can initiate cavitation under reduced acoustic pressures.

Acoustic cavitation inception by nanoparticles was tested as reported previously.[29, 49] Briefly, samples were placed in a plastic tube with low acoustic attenuation with the center of the sample aligned with a focused HIFU transducer in the z-direction, while the generated echogenic bubbles were detected using a phased array scanning probe operating at 1.5 MHz in Cadence Contrast Pulse Sequencing (CPS) mode[11] in the x–y plane (Figure S2). Initially, we detected the threshold peak negative pressure for generation of ultrasound responsive bubbles (*i. e.* detectable contrast enhancement by the scanning probe) by increasing the applied peak negative pressure stepwise from 3 to 22 MPa, in pulse packets of 12 sine waves at a repetition rate of 10 Hz. The lowest peak negative pressure value that gave detectable ultrasound response was recorded as the threshold pressure. All nanoparticles dispersed in ultrapure water were tested at two different particles concentrations that gave detectable signal in our previous studies;[29, 49] 10^{11} particles mL^{-1} and 4×10^{11} particles mL^{-1} (distilled, tap, or degassed ultrapure water were also used without noticeable differences; see below). Particle concentrations were adjusted in accordance with initial concentrations measured by NTA (Table 1). At the particle concentration of 10^{11} particles mL^{-1}, only MCM-48R produced ultrasound responsive bubbles, observed as bright spots in the ultrasonograph (Video S1) with a threshold pressure around 6.2 MPa. Other particles did not produce any response even at the highest pressure of 22 MPa used in this study (Table 2). Also, it is important to note that in the absence of nanoparticles or HIFU exposure, no signal was observed. Increasing the particle concentration 4-fold to 4×10^{11} particles mL^{-1} did not affect the peak negative pressure threshold for MCM-48R. At this particle concentration slight response was observed for MCM-48S (with smooth surface) at pressures higher than 9.1 MPa, but this response was much weaker than that generated by the rough MCM-48R particles. Also, acoustic cavitation was observed for Random at this high particle concentration at pressures above 6.2 MPa (Table 2), but signal dies off very quickly in ~2 s (Figure S3 and Video S2). For comparison, the response of MCM-48R was measured for 13 min under continuous HIFU exposure and considerable response was observed even after 5 min of HIFU insonation (Figure S4 and Video S1). The short-lived response of Random suggests that these particles can stabilize only a few nanobubbles capable of nucleating acoustic cavitation at the applied experimental conditions. On the other hand, for MCM-48R there should be large number of stabilized nanobubbles to produce ultrasound responsive bubbles for around 5 min under continuous HIFU insonation. Also, it should be noted that the bright spots immediately disappeared right after turning off the HIFU exposure (Video S1) due to the short lifetime of free gas bubbles in water.[9]

Still images of typical responses of the nanoparticles under HIFU insonation (peak negative pressure was 10.6 MPa for responsive particles and 22 MPa for non-responsive particles) at both particle concentrations are given in Figure 2a. To quantify the response generated by the particles, three 15 s videos were recorded for each sample. Videos were analyzed using MATLAB (Mathworks, Inc.) to calculate the total intensity of the bright spots (*i. e.* integrated pixel intensity of the region of interest from the acquired 15 s videos); see Video S1 for a typical response generated by MCM-48R. Figure 2a shows the total intensities generated by each particle. Statistically significant signal generation was only observed for

MCM-48R (at both concentrations) and MCM-48S (only at the high particle concentration). Interestingly, increasing the particle concentration decreased the total intensity for MCM-48R. We believe that this is because of the increased rate of destruction of the generated bubbles by the increased number acoustic cavitation events. In fact, still images in Figure 2a show that at the high particle concentration signal concentrated in a smaller area, which is probably due to the destruction of the bubbles before they diffuse out the focus region of the HIFU.

The effect of MCM-48R particle concentration on the total generated intensity was investigated by gradually decreasing the particle concentration from 10^{11} particles mL^{-1} to ~10^{10} particles mL^{-1} (Figure 3a) at the peak negative pressure of 10.6 MPa. Gradual decrease in the response with decreasing particle concentration was observed and it was found that the total intensity of MCM-48R the acoustic signal was statistically different than background down to a particle concentration down to 1.25×10^{10} particles mL^{-1}. Highest ultrasound response was observed at 10^{11} particles mL^{-1}; increasing particle concentration to 4×10^{11} particles mL^{-1} decreased the total intensity as discussed above. We also investigated the effect of peak negative pressure on the generated total intensity by MCM-48R at the particle concentration of 10^{11} particles mL^{-1} (Figure 3b). It was observed that increasing the peak negative pressure from 6.2 to 10.6 MPa sharply improved the response, but increasing it further up to 22 MPa did not significantly affect the total intensity. Accordingly, particle concentration of 10^{11} particles mL^{-1} and peak negative pressure of 10.6 MPa was determined as optimum conditions and used in the rest of the study, unless otherwise specified.

The effect of water source on the total intensity was studied using different kinds of water: ultrapure, distilled, tap, and degassed ultrapure water (ultrapure was degassed by heating it until boiling, distilled and tap waters were not degassed), with and without MCM-48R, since the impurities and dissolved gas can also nucleate acoustic cavitation (Figure S5).[36] There was no statistically significant change in the responsivity of MCM-48R when dispersed in different media. More importantly, no response was observed in the absence of the particles, indicating that contaminants common to water sources cannot stabilize nanobubbles for observable acoustic cavitation without addition of MCM-48R in the experimental condition used here (peak negative pressure of 10.6 MPa and 12 cycles). The stability of the nanobubbles was investigated by incubating the MCM-48R in ultrapure water at RT. It was observed that responsivities of the particles stored for 3 d or 14 d were almost same with the fresh particles (see the Supporting Information, Figure S6) suggesting that the nanobubbles are stable for at least two weeks, which is in accordance with our previous findings with Pluronic F127 stabilized hydrophobic MCM-41 MSNs.[29]

To understand the effect of chemical structure on acoustic cavitation by porous nanoparticles, we examined the particles by Fourier Transform Infrared (FTIR) Adsorption Spectroscopy and Thermal Gravimetric Analysis (TGA). FTIR spectra of the silica nanoparticles (Figure 4) revealed that each of the mesoporous silica nanoparticles contained some amount of carbon impurities such as remaining surfactants and non-hydrolyzed ethoxy groups (the multiple peak between 2800 cm^{-1} and 3050 cm^{-1}), which is especially high for responsive MCM-48 type MSNs. The high carbon impurity content of these MSNs can be

caused by the high surfactant amount used in their synthesis and/or their narrow and bended pore structure, which can hinder the removal of surfactant molecules. Interestingly, the carbon impurity pattern of the Random shows an intense peak at around 2850 cm^{-1}, which is different than the other particles. This peak is attributed to the remaining ethoxy groups from incomplete hydrolysis of TEOS, which can be expected for the particles prepared at neutral pH. Other than residual carbon, FTIR spectra of the particles give evidence about the condensation degree of silica network, abundance of silanol groups, and internal stress of the silica network.[50–55] The broad peak between 3000 cm^{-1} and 3600 cm^{-1} in the FTIR spectra is assigned to the interacting hydroxyl groups (i. e. germinal and vicinal) and the narrow peak around 3750 cm^{-1} is assigned to the isolated hydroxyl groups.[50] Therefore, a more intense isolated hydroxyl peak suggests a silica network with fewer hydroxyl groups (*i.e.* more condensed silica network with more siloxane bonds) since there should be more hydroxyl free areas to get isolated hydroxyl groups.[54] The isolated hydroxyl peak was more pronounced for MCM-48 type of particles, especially for MCM-48R. The broad band between 1000 and 1300 cm^{-1} is the asymmetric Si-O-Si stretching. The position of the main peak at around 1100 cm^{-1} can give insight about how crosslinked the silica network is; higher wavenumber (*i. e.* lower wavelength) means that higher energy required for stretching, which suggests silica network with a higher crosslinking degree.[51–53] According to the position of this band, dendritic and MCM-48 type of particles has more crosslinked silica network than the other particles which also indicates more condensed silica network with less hydroxyl groups (Figure 4b).

To further explore the types of surface functionalities such as carbon impurities on the nanoparticles, thermogravimetric analysis (TGA) was performed (Figure 5). The particles were gradually heated to 850 °C, during which the measured weight loss for silica particles originated from the dehydroxylation of the silica network and decomposition of carbon impurities.[50] The TGA curves of the silica nanoparticles can be roughly divided into three regions: i) 50–150 °C: removal of adsorbed water and remaining solvents; ii) 150–600 °C: decomposition of carbon impurities and removal of interacting hydroxyl groups; and iii) >600 °C: removal of isolated hydroxyl groups.[50] In the second (carbon impurity) region, a weight decrease of ~6.5% was observed for MCM-41, while weight losses of ~15% and ~11.5% were measured for MCM-48S and MCM-48R, respectively. The higher weight loss for MCM-48 type of particles is due to higher carbon impurity contents of these nanoparticles, in accordance with FTIR spectroscopy. In the third region, highest weight loss (~3.5%) was observed for MCM-48R, suggesting a higher isolated hydroxyl content of these particles, which was also confirmed by FTIR.

Next, the chemical origin of nanobubble stabilization was explored by comparing structure and ultrasound contrast before and after chemical treatment. To entrap a stable gas nanobubble in a cavity, there must be some resistance against the movement of the three-phase line through bottom of the cavity. Such resistance presents as contact angle hysteresis, or the difference between advancing and receding contact angles of water on cavity wall. A higher contact angle hysteresis indicates a more stable three-phase line at each pore wall, and thus nanoparticles with higher hysteresis provide better nanobubble stabilization.[37, 39] Also, water contact angles at the cavity walls close to or larger than 90° are required to stabilize the entrapped gas. For these cases, R of the water contact line is very large or

negative, which yields negligible or no interfacial tension and makes the entrapped bubble stable (see above for the explanation based on Laplace pressure equation). According to FTIR and TGA results, both carbon impurities and siloxane rich surfaces of MCM-48R can provide the required hydrophobic cavity walls for nanobubble stabilization. To identify the origin of the hydrophobicity in these nanoparticles, we further purified the MCM-48R to remove carbon impurities by refluxing in acidic ethanol or calcining at 550 °C for 2 h. The intensity of the carbon impurity peak was significantly reduced after acidic ethanol treatment and it completely disappeared after calcination (Figure 6). Also, acidic ethanol treatment did not significantly affect the isolated hydroxyl peak at 3750 cm^{-1}, but calcination significantly intensified this peak, indicating the dehydroxylation of the surface and generation of relatively hydrophobic siloxane groups.[56] In addition, the intensity of the Si-OH stretching peak at around 950 cm^{-1} was reduced after calcination but not after acidic ethanol treatment, which also indicates the dehydroxylation of the silica surface after calcination. Figure 6c compares the ultrasound contrast generated by the as-prepared, acidic ethanol treated, and calcined MCM-48R. Refluxing in acidic ethanol (which partially removed the carbon impurities) was resulted in a slight decrease in the response of the MCM-48R. On the other hand, after calcination the ultrasound response completely quenched, suggesting that carbon impurities are the main source hydrophobicity and plays a crucial role in stabilization of nanobubbles by the nanoparticles.

Based on these characterizations, it is not clear if acoustic cavitation is nucleated by the surface nanobubbles or the gas entrapped inside the pores. To explore this, we first prepared two additional MCM-48 nanoparticles with methyl modified and unmodified pore walls. First, MCM-48S cores were prepared by condensation of 0.8 mL of TEOS, followed by another 0.3 mL of TEOS to form rough surface around the particles (MCM-48D; see Experimental Section for details). To investigate the effect of hydrophobic modification of the pores, methyltrimethoxysilane (MTMS) was added in between the two TEOS addition steps (MCM-48MD). According to TEM and NTA, both the MCM-48MD and MCM-48D have sizes around 100 nm with narrow size distribution and good dispersibility in water (Figure 7, Figure S7, Table S1). It is important to note that methyl modification has no significant effect on the dispersibility of the particles in water because of the outer silica layer. Also, these particles have smoother surfaces than MCM-48R, presumably due to the lower TEOS content in the synthesis of these particles. FTIR spectra (Figure S8) of the nanoparticles showed that both MCM-48D and MCM-48MD contain similar carbon impurities as MCM-48S and MCM-48R. Also, the peak at around 1300 cm^{-1} in the FTIR spectrum of MCM-48MD can be assigned to the methyl groups of this particle, which proves the methyl modification. Figure 8 shows the total intensity generated by MCM-48D and MCM-48MD at the particle concentration of 10^{11} particles mL^{-1} and at different peak negative pressures. A lower threshold pressure observed for methyl modified MCM-48MD showing that hydrophobic modification of the pores improves the responsivity (*i. e.* ability of stabilization nanobubbles). Nevertheless, without hydrophobic modification of the pores there was still remarkable ultrasound response.

To further evaluate the role of nanobubbles on the surface of the nanoparticles and gas entrapped inside the pores, we treated MCM-48R and MCM-48MD with ethanol and/or bovine serum albumin (BSA). Ethanol is expected to destroy both surface and inner bubbles

by wetting both the surface and the pores of the nanoparticles and exchanging with the entrapped gas.[29] But BSA can only destroy the surface nanobubbles because this large molecule (~7 nm) cannot penetrate inside the small pores of the MCM-48 type MSNs (~3 nm).[44] For this, the nanoparticles were mixed with BSA prior to acoustic cavitation experiments. It is well-known that when nanoparticles are introduced into a protein solution, their surfaces are immediately covered by proteins.[57, 58] BSA can adsorb to almost any surface because of its hydrophobic and hydrophilic structure, therefore it can be expected that BSA will associate with the hydrophobic regions of the nanoparticle surface and make it hydrophilic to prevent nanobubble stabilization on these cavities. Accordingly, we stirred the MCM-48R or MCM-48MD in BSA solution (50 mg mL^{-1}) for 2 h to form a BSA corona around the particles, and we centrifuge washed the particles to remove excess BSA. It was observed that after formation of the BSA corona around the MCM-48MD, the total intensity was reduced by about 85% (Figure 9), though the signal was still distinguishable from background (Figure 9a). The reduction in the total intensity for BSA coated MCM-48R, on the other hand, was only about 45%. However, addition of 90% v/v ethanol completely quenched the responsivity of both MCM-48R and MCM-48MD with or without BSA coating (Figure 9). These results suggest that acoustic cavitation is initiated mostly by the surface nanobubbles, which are mostly larger than the size of BSA (~7 nm). The contribution of such larger surface nanobubbles are more pronounced for MCM-48MD, most probably due to its smoother surface. On the other hand, the rough surface of MCM-48R can entrap more small surface nanobubbles that are not accessible to the large BSA molecules. The data also suggest that small cavities (smaller than the size of single BSA molecule), possibly inside the pores or at the pore openings, can also facilitate acoustic cavitation since significant response was observed for both nanoparticles after BSA corona formation.

DISCUSSION

Recently, it has been shown that nanobubbles stabilized by nanoparticles (silica, polystyrene and PTFE) with various morphologies (porous, solid, cup-shaped etc.) can initiate acoustic cavitation of water, which allows development of nanoscale agents for ultrasound imaging and therapy.[28–33] For example, Zhang et al.,[28] prepared hydrophobic MSN and capped them with cyclodextrin to make the hydrophobic MSN dispersible in water. They observed an increase in the concentration of reactive oxygen species when the hydrophobic MSN insonated with low energy ultrasound, which is consistent with cavitation. Later, the same group obtained similar results using bare MSNs without any hydrophobic modification.[32] While in these studies there was no direct observation of acoustic cavitation, authors concluded that the air encapsulated inside the pores initiates acoustic cavitation and reactive oxygen species are produced as a result. More recently, we showed that acoustic cavitation initiated by Pluronic polymer stabilized hydrophobic MSN, when exposed to HIFU, can be observed by using a conventional imaging transducer.[29] In these studies it was assumed that the air encapsulated inside the mesopores of silica nanoparticles initiates acoustic cavitation. Later, it was shown that the air stabilized inside the cavities of nanocups[30, 33] or even at the surface of solid hydrophobic particles[31] can also initiate acoustic cavitation. Here, we prepared several MSNs with different morphologies and without any hydrophobic

modification (expect MCM-48MD) and observed that acoustic cavitation inception by only MCM-48 type of MSNs but not for the others (MCM-41, Dendritic, Random).

These results raise several questions about the nanobubble stabilization by mesoporous silica nanoparticles. First of all, what is the origin of hydrophobicity of unfunctionalized “bare” mesoporous silica nanoparticles that provides the stabilization of gas bubbles inside the cavities? The chemical formula of silica nanoparticles is often expressed simply as SiO_2, the chemical structure of amorphous silica prepared by sol-gel methods is much more complicated than this. Due to the incomplete condensation of silica, it should be written as $SiO_{2-n}(OH)_{2n}$. Since siloxane bonds are more hydrophobic than silanol groups, the ratio of these two groups determines the contact angle of the particles at the air-water interface. In fact, contact angles above 90° have been both theoretically and experimentally demonstrated for highly dehydroxylated silica surfaces.[56, 59] In addition, there may be alkoxy groups in the final structure remaining from the incomplete hydrolysis of the alkoxysilane monomer, which can add hydrophobicity to the particles. Furthermore, for mesoporous particles the residual surfactant molecules can be present in the purified particles, which can create local hydrophobic regions or increase contact angle hysteresis. Finally, depending on the synthesis conditions, different siloxane rings (4, 5, 6 membered etc.) with different activities can be obtained[60] but this is beyond the scope of this study. Such differences between silica nanoparticles prepared in this study were clearly observed in the FTIR and TGA data (Figures 4 and 5). The MCM-48-type nanoparticles that showed greater nucleation of acoustic cavitation exhibited a more condensed silica network with a large amount of carbon impurities. Further purification of the particles by calcination completely quenched responsivity of the particles, suggesting that carbon impurities help the nanobubble stabilization by making the walls of pores and/or surface grooves and pits more hydrophobic. However, number of siloxane groups on the particle surface appeared to have no significant effect on the responsivity of the MCM-48R (Figure 6).

The second question is whether the acoustic cavitation is initiated by nanobubbles stabilized at the nanoparticle surface or inside the pores? Unfortunately, it is a very challenging to image the nanobubbles stabilized on the nanoparticles or inside their pores; to our knowledge, there is no conventional method to do this. Nevertheless, the effects of BSA and ethanol addition (Figure 9) showed that the acoustic cavitation is mostly initiated by nanobubbles stabilized at the surface, which should have sizes larger than the size of a BSA protein (~7 nm diameter).[61] Thus, is nanoporosity really needed for initiation of the acoustic cavitation? The data presented in this study and previous findings of Jin et al.,[31] with solid PTFE nanoparticles indicates that it is not critical; the air stabilized in the narrow pores of MSNs (2–3 nm) has no direct role in the acoustic cavitation inception. It appears to be initiated mostly by surface bubbles. Nevertheless, it is believed that pore openings can help the stabilization of surface nanobubbles by addition of surface roughness and potentially formation of a Cassie state.[62] In addition, the gas stored inside the pores can contribute to the growth and merging of surface bubbles.

On this subject, what is the role of surface roughness? Previous studies with microparticles[63–65] demonstrated that rough particles can initiate acoustic cavitation at much lower pressures than their smooth counterparts. Apparently, surface roughness creates

suitable cavities for the stabilization of nanobubbles on the surface of microparticles. Our initial results with six different kinds of silica nanoparticles (Figure 2 and Table 2) also demonstrated a similar trend, as only rough MCM-48R could initiate the acoustic cavitation at the particle concentration of 10^{11} particles mL^{-1} in our experimental conditions. However, later results with MCM-48D and MCM-48MD (Figure 8) showed that although these particles had smoother surfaces than MCM-48R, they had similar responsiveness. In addition, Jin et al.,[31] observed acoustic cavitation inception by fairly smooth PTFE nanoparticles at experimental conditions similar to ours. We believe the difference in the results obtained with microparticles and nanoparticles is due to pore size scaling, as cavities of ~100 nm were observed for microparticles but the cavities in this study were much smaller. Therefore, the size of nanobubbles stabilized on the surface of nanoparticles can be larger than the size of surface cavities since nanobubbles can be stabilized by multiple cavities on rough and hydrophobic nanoparticle surface. Nevertheless, BSA coating experiments (Figure 9) showed that after coating the rough nanoparticles with BSA, some nanobubbles remain on the surface of these rough nanoparticles (probably inside the cavities smaller than the size of BSA; ~7 nm) and these small nanobubbles are able to nucleate acoustic cavitation.

Finally, what is the effect of hydrophilic surface modification on the responsivity of the particles? While hydrophobicity is required for stabilization of nanobubbles, modification of the nanoparticle surface with hydrophilic molecules (*e. g.* PEG, phospholipids, peptides) is required prior to their in vivo administration to prevent aggregation in biological media, reduce complement activation, and potentially promote targeting to a diseased region. Hydrophilic modification surface modification can destabilize nanobubbles and accordingly the responsivity of the nanoparticles. In fact, coating the particles with hydrophilic BSA significantly quenched the response generated by the nanoparticles, especially for MCM-48MD (Figure 9). Nevertheless, there was still strong response for BSA coated MCM-48R (~55% of the initial response). In addition, in our previous work[29] we reported that Pluronic polymer stabilized hydrophobic MCM-41 MSNs produced easily detectable response when insonated with HIFU, which indicates that a very hydrophobic surface (*i. e.* not dispersible in water in the absence of amphiphilic molecules) can resist coating by macromolecules, thereby preserving its responsiveness. These results indicate that although after hydrophilic surface modification a decrease in the responsivity of the hydrophobic nanoparticles can be expected, it is still possible to design nanoscale ultrasound agents with good responsivity by engineering the surface roughness and interfacial hydrophobicity.

CONCLUSIONS

In conclusion, to understand the nanobubble stabilization process by porous silica nanoparticles and acoustic cavitation initiated by these stabilized nanobubbles, we prepared several spherical silica nanoparticles with sizes around 100 nm but with different morphologies. FTIR and TGA analyses of the nanoparticles revealed that nanoparticles have very distinct compositions, with varying amounts of carbon impurities, hydroxyl content, and degrees of silica crosslinking, even if prepared using the same monomer (TEOS) and surfactant (CTAB). To study the acoustic cavitation inception by nanoparticles, nanoparticle samples at different concentrations were insonated with HIFU at different peak negative

pressures. It was found that only MCM-48 type MSNs initiated acoustic cavitation in our experimental conditions, which is due to their more hydrophobic and rougher surfaces. However, additional purification steps (acidic ethanol treatment and calcination) and additives (ethanol and BSA) were found to destabilize the nanobubbles. These experiments suggested that for rough particles acoustic cavitation is mostly initiated by the large nanobubbles (>7 nm), which are stabilized on the partially hydrophobic surface of the mesoporous silica nanoparticles. However, for rough and highly hydrophobic nanoparticle interfaces the intrusion of macromolecules can be resisted due to sterics. We believe the results presented in this paper can provide useful information to the researcher to design nanoscale (<100 nm) ultrasound agents for imaging and therapy purposes.

MATERIALS AND METHODS

Materials

Tetraethyl orthosilicate (TEOS), cetyltrimethylammonium bromide (CTAB), and triethanol amine were purchased from Across Organics. Methyltrimethoxysilane (MTMS) was purchased from TCI Chemicals. Pluronic F127 polymer was purchased from Anatrace, Inc. Ethanol was purchased from Decon Laboratories. Ammonium nitrate, hydrochloric acid (HCl, 37%) and cyclohexane were purchased from Fisher Scientific. Sodium hydroxide and ammonium hydroxide solution (28–30%) were purchased from Macron Chemicals. Bovine serum albumin (BSA) was purchased from USBiological Life Sciences. All materials were used as received.

Synthesis of MCM-41

The MCM-41 type MSNs was synthesized according to a previous report.[43] CTAB (200 mg) and Pluronic F127 polymer (6 mg) were dissolved in ultrapure water (96 mL) and 2 M NaOH (0.7 mL) was added. The reaction solution was heated to 80 °C while stirring at 600 rpm. 1.5 mL of TEOS to this solution the reaction solution was kept at the same condition for 3 h.

Synthesis of MCM-48S and MCM-48R

The MCM-48 type MSNs was synthesized by slightly modifying a previous report.[44] CTAB (250 mg) and Pluronic F127 polymer (1 g) were dissolved in ultrapure water (45 mL) and ethanol (20 mL) and 4.5 mL of ammonium hydroxide solution (28–30%) was added. The reaction mixture was stirred vigorously at 40 °C for 15 min. TEOS (0.8 mL for MCM-48S and 1.6 mL for MCM-48R) was rapidly added to this solution and reaction mixture was kept at same conditions for 2.5 h.

Synthesis of Dendritic

The MSN with dendritic pore structure was prepared by slightly modifying a previous report.[46] CTAB (1.3 g) and triethanol amine (45 mg) was dissolved in ultrapure water (15 mL) at 60 °C while stirring at ~150 rpm. TEOS (0.5 mL) was dissolved in 4.5 mL of cyclohexane and slowly added on top of the water phase. Then the temperature increased to 70 °C and reaction mixture was kept at this condition for 8 h.

Synthesis of Random

The MSN with non-organized pore structure was prepared by modifying a previous report.[45] CTAB (200 mg) was dissolved in 70 mL of PBS (pH 7.4, 10 mM) at 65 °C while stirring at 600 rpm. TEOS (1 mL) was rapidly added to this solution and reaction mixture was kept at same conditions for 3 h.

Synthesis of Solid

Solid silica nanoparticles was prepared according to Stober method.[47] ultrapure water (0.5 mL), ethanol (20 mL) were mixed with 6 mL of ammonium hydroxide solution (28–30%). Then, TEOS (3 mL) was dissolved in 80 mL of ethanol was gently added onto this solution. The reaction mixture was stirred (300 rpm) at room temperature for 13 h.

Synthesis of MCM-48D and MCM-48MD

For synthesis of MCM-48D, CTAB (250 mg) and Pluronic F127 polymer (1 g) were dissolved in ultrapure water (45 mL) and ethanol (20 mL) and 4.5 mL of ammonium hydroxide solution (28–30%) was added. The reaction mixture was stirred vigorously at 40 °C for 15 min. TEOS (0.8 mL) was rapidly added to this solution and reaction mixture was stirred at 40 °C for 1.5 h. Then, TEOS (0.3 mL) in ethanol (1 mL) was added and reaction mixture was further kept at same condition for 1 h. For synthesis of MCM-48MD, 0.18 mL of MTMS (dissolved in 0.8 mL of ethanol) was added 5 min after the first TEOS addition, other parameters were same with the MCM-48D synthesis.

Purification of the nanoparticles

All nanoparticles were collected by centrifugation (7000 rcf) and washed with ethanol twice. To extract surfactant molecules from MSNs, nanoparticles were dispersed in ethanolic ammonium nitrate solution (20 mg mL^{-1}) and vigorously stirred at 60 °C for at least 30 min. Then, nanoparticles were collected by centrifugation (7000 rcf) and ammonium nitrate treatment was repeated for one more time. Finally, nanoparticles were washed with ethanol twice and dried at 65 °C for overnight. The dried nanoparticles were stored at room conditions.

Acidic ethanol treatment of MCM-48R

To further purify MCM-48R, 10 mg of MCM-48R was dispersed in 20 mL of ethanol and 0.25 mL HCl (37%) was added dropwise and vigorously stirred at 65 °C for 2 h. Then, nanoparticles were collected by centrifugation (7000 rcf) and acidic ethanol treatment was repeated for one more time. Finally, nanoparticles were washed with ethanol twice and dried at 65 °C overnight.

Calcination of MCM-48R

To completely remove the carbon impurities, 10 mg of MCM-48R was heated to 550 °C at a ramping rate of 5 °C min^{-1} and kept at this temperature for 2 h. Then, nanoparticles were slowly cooled down to the room temperature.

Coating MCM-48MD with BSA

4 mg of MCM-48MD was dispersed in 2 mL of ultrapure water and mixed with 2 mL of BSA solution in water (100 mg mL^{-1}). The solution was sonicated for ~1 min and stirred at 500 rpm for 2 h. Then nanoparticles were collected by centrifugation (7000 rcf) and washed with water to remove excess BSA.

Acoustic cavitation experiments and analysis

Ultrasound experiments were performed according to our previous reports.[29, 49] Briefly, a spherically focused, single-element, HIFU transducer (Sonic Concepts H101, 64.0 mm Active Diameter × 63.2 mm Radius of Curvature) was equipped with a coupling cone (Sonic Concepts C101) was used for HIFU exposure. Prior to the experiments, the transducer was submerged in a water tank and it was connected to a 30 MHz Function/Arbitrary Waveform Generator (Agilent Technologies) via an AG Series Amplifier (T&C Power Conversion, Inc.), the amplifier operating at 100% output. Different peak to peak voltages between 0.3 and 2 V were applied and the corresponding peak pressures was measured via needle hydrophone calibration (HNC-0200, Onda Corp.), which were found to be in the range of ~3–22 MPa. In a typical experiment, nanoparticles were dispersed in water (1 mL) at different concentrations between 10^{10} and 4×10^{11} particles mL^{-1} and put into a plastic bulb. The plastic bulb was positioned on top of the coupling cone to guarantee proper HIFU focusing into the center of the sample. A vector array 4V1 (Acuson) transducer (1–4 MHz), which was connected to a Siemens Acuson Sequoia C512 scanner operating in CPS mode at 1.5 MHz, a mechanical index (MI) of 0.19 and a frame rate of 14 Hz, was aligned to acquire horizontal cross-sectional images of the sample (Figure S2). To align the imaging transducer to the focus of HIFU, the transducer was placed at a distance of approximately 1 cm from the plastic sample bulb and the horizontal position of the transducer was manually adjusted until the maximum contrast was obtained. Then, HIFU was applied using the following Waveform Generator settings: Vpp between 0.3 and 2 V, 1.1 MHz center frequency, 0.1 s pulse interval (burst period), and 12 cycles. During the HIFU application, the videos were recorded by the Siemens Acuson Sequoia C512 scanner for 15 s. MATLAB (Mathworks, Inc.) code which calculates the total intensity of the bright spots in the region of interest of each frame of the videos, was used to analyze the videos.

Characterization

Transmission electron microscopy (TEM) images of the nanoparticles were taken using a CM 100 (Philips) microscope. The concentration and size distribution of the nanoparticles dispersed in water were determined via Nanoparticle Tracking Analysis by using a NanoSight LM10 setup (Malvern). FTIR spectra of the nanoparticles were collected by using a Fourier transform infrared spectrometer (Nicolet 6700, Thermo Scientific) which is equipped with a Diffuse Reflectance Accessory. Thermal gravimetric analyses (TGA) of the nanoparticles were performed using a Pyris 1 TGA (Perkin Elmer) under nitrogen atmosphere.

Supplementary Material

Refer to Web version on PubMed Central for supplementary material.

Acknowledgments

Funding Sources

This work was supported by NIH (Grant Nos. DP2EB020401, R21EB018034, and R00CA153935).

The authors thank Prof. Jeffrey Stansbury for use of his Thermo Scientific Nicolet 6700 FTIR and Perkin Elmer Pyris 1 TGA, Prof. Mark A. Borden for use of his Onda HNC-0200 needle hydrophone, and Dr. Parag Shah for his help with the FTIR and TGA measurements.

REFERENCES

1. Kiessling F, Fokong S, Bzyl J, Lederle W, Palmowski M, Lammers T. Recent advances in molecular, multimodal and theranostic ultrasound imaging. Adv. Drug Delivery Rev. 2014; 72:15–27.
2. Jain RK, Stylianopoulos T. Delivering nanomedicine to solid tumors. Nature Rev. Clin. Oncol. 2010; 7(11):653–664. [PubMed: 20838415]
3. Cai WB, Chen XY. Nanoplatforms for targeted molecular imaging in living subjects. Small. 2007; 3(11):1840–1854. [PubMed: 17943716]
4. Manthe RL, Foy SP, Krishnamurthy N, Sharma B, Labhasetwar V. Tumor Ablation and Nanotechnology. Mol. Pharm. 2010; 7(6):1880–1898. [PubMed: 20866097]
5. Leinenga G, Goetz J. Scanning ultrasound removes amyloid-beta and restores memory in an Alzheimer's disease mouse model. Sci. Trans. Med. 2015; 7(278):278ra33.
6. Lentacker I, De Cock I, Deckers R, De Smedt SC, Moonen CTW. Understanding ultrasound induced sonoporation: Definitions and underlying mechanisms. Adv. Drug Delivery Rev. 2014; 72:49–64.
7. Unga J, Hashida M. Ultrasound induced cancer immunotherapy. Adv. Drug Delivery Rev. 2014; 72:144–153.
8. Hynynen K. Ultrasound for drug and gene delivery to the brain. Adv. Drug Delivery Rev. 2008; 60(10):1209–1217.
9. Schutt EG, Klein DH, Mattrey RM, Riess JG. Injectable microbubbles as contrast agents for diagnostic ultrasound imaging: The key role of perfluorochemicals. Angew. Chem. Int. Ed. 2003; 42(28):3218–3235.
10. Luke GP, Hannah AS, Emelianov SY. Super-Resolution Ultrasound Imaging in Vivo with Transient Laser-Activated Nanodroplets. Nano Lett. 2016; 16(4):2556–2559. [PubMed: 27035761]
11. Phillips P, Gardner E. Contrast-agent detection and quantification. Eur. Radiol. 2004; 14:P4–P10. [PubMed: 15700327]
12. Yang P, Wang F, Luo XF, Zhang YT, Guo J, Sho WB, Wang CC. Rational Design of Magnetic Nanorattles as Contrast Agents for Ultrasound/Magnetic Resonance Dual-Modality Imaging. ACS Appl. Mater. Interfaces. 2014; 6(15):12581–12587. [PubMed: 25022424]
13. Song S, Guo HZ, Jiang ZQ, Jin YQ, Zhang ZF, Sun K, Dou HJ. Self-Assembled Fe3O4/Polymer Hybrid Microbubble with MRI/Ultrasound Dual-Imaging Enhancement. Langmuir. 2014; 30(35): 10557–10561. [PubMed: 25136957]
14. Hu H, Zhou H, Du J, Wang ZQ, An L, Yang H, Li FH, Wu HX, Yang SP. Biocompatiable hollow silica microspheres as novel ultrasound contrast agents for in vivo imaging. J. Mater. Chem. 2011; 21(18):6576–6583.
15. Martinez HP, Kono Y, Blair SL, Sandoval S, Wang-Rodriguez J, Mattrey RF, Kummel AC, Trogler WC. Hard shell gas-filled contrast enhancement particles for colour Doppler ultrasound imaging of tumors. MedChemComm. 2010; 1(4):266–270. [PubMed: 21841967]
16. Yang P, Zhao F, Ding J, Guo J, Shi W, Wang C, Hu X. Bubble-in-Bubble Strategy for High-Quality Ultrasound Imaging with a Structure Coupling Effect. Chem. Mater. 2014; 26(6):2121–2127.
17. An L, Hu H, Du J, Wei J, Wang L, Yang H, Wu DM, Shi HL, Li FH, Yang SP. Paramagnetic hollow silica nanospheres for in vivo targeted ultrasound and magnetic resonance imaging. Biomaterials. 2014; 35(20):5381–5392. [PubMed: 24703718]

18. Nakatsuka MA, Hsu MJ, Esener SC, Cha JN, Goodwin AP. DNA-Coated Microbubbles with Biochemically Tunable Ultrasound Contrast Activity. Adv. Mater. 2011; 23(42):4908–4912. [PubMed: 21956383]
19. Wang C-H, Huang Y-F, Yeh C-K. Aptamer-Conjugated Nanobubbles for Targeted Ultrasound Molecular Imaging. Langmuir. 2011; 27(11):6971–6976. [PubMed: 21553884]
20. Yin T, Wang P, Li J, Zheng R, Zheng B, Cheng D, Li R, Lai J, Shuai X. Ultrasound-sensitive siRNA-loaded nanobubbles formed by hetero-assembly of polymeric micelles and liposomes and their therapeutic effect in gliomas. Biomaterials. 2013; 34(18):4532–4543. [PubMed: 23522375]
21. Sirsi SR, Borden MA. Advances in Ultrasound Mediated Gene Therapy Using Microbubble Contrast Agents. Theranostics. 2012; 2(12):1208–1222. [PubMed: 23382777]
22. Fan CH, Ting CY, Lin HJ, Wang CH, Liu HL, Yen TC, Yeh CK. SPIO-conjugated, doxorubicin-loaded microbubbles for concurrent MRI and focused-ultrasound enhanced brain-tumor drug delivery. Biomaterials. 2013; 34(14):3706–3715. [PubMed: 23433776]
23. Zhao YZ, Du LN, Lu CT, Jin YG, Ge SP. Potential and problems in ultrasound-responsive drug delivery systems. Int. J. Nanomed. 2013; 8:1621–1633.
24. Aryal M, Vykhodtseva N, Zhang YZ, McDannold N. Multiple sessions of liposomal doxorubicin delivery via focused ultrasound mediated blood-brain barrier disruption: A safety studyle. J. Controlled Rel. 2015; 204:60–69.
25. Mitragotri S. Innovation - Healing sound: the use of ultrasound in drug delivery and other therapeutic applications. Nat. Rev. Drug Discov. 2005; 4(3):255–260. [PubMed: 15738980]
26. Mitragotri S, Blankschtein D, Langer R. Ultrasound-mediated transdermal protein delivery. Science. 1995; 269(5225):850–853. [PubMed: 7638603]
27. Stylianopoulos T, Jain RK. Design considerations for nanotherapeutics in oncology. Nanomedicine. 2015; 11(8):1893–1907. [PubMed: 26282377]
28. Zhao Y, Zhu Y, Fu J, Wang L. Effective Cancer Cell Killing by Hydrophobic Nanovoid-Enhanced Cavitation under Safe Low-Energy Ultrasound. Chem. Asian. J. 2014; 9(3):790–796. [PubMed: 24339016]
29. Yildirim A, Chattaraj R, Blum NT, Goldscheitter GM, Goodwin AP. Stable Encapsulation of Air in Mesoporous Silica Nanoparticles: Fluorocarbon-Free Nanoscale Ultrasound Contrast Agents. Adv. Healthcare Mater. 2016; 5(11):1290–1298.
30. Kwan JJ, Graham S, Myers R, Carlisle R, Stride E, Coussios CC. Ultrasound-induced inertial cavitation from gas-stabilizing nanoparticles. Phys. Rev. E. 2015; 92(2):5.
31. Jin QF, Kang ST, Chang YC, Zheng HR, Yeh CK. Inertial cavitation initiated by polytetrafluoroethylene nanoparticles under pulsed ultrasound stimulation. Ultrason. Sonochem. 2016; 32:1–7. [PubMed: 27150739]
32. Zhao Y, Zhu YC. Synergistic cytotoxicity of low-energy ultrasound and innovative mesoporous silica-based sensitive nanoagents. J. Mater. Sci. 2014; 49(10):3665–3673.
33. Kwan JJ, Myers R, Coviello CM, Graham SM, Shah AR, Stride E, Carlisle RC, Coussios CC. Ultrasound-Propelled Nanocups for Drug Delivery. Small. 2015; 11(39):5305–5314. [PubMed: 26296985]
34. Zhang L, Belova V, Wang HQ, Dong WF, Mohwald H. Controlled Cavitation at Nano/Microparticle Surfaces. Chem. Mater. 2014; 26(7):2244–2248.
35. Morch KA. Cavitation nuclei and bubble formation - A dynamic liquid-solid interface problem. J. Fluid Eng.-T ASME. 2000; 122(3):494–498.
36. Morch KA. Cavitation inception from bubble nuclei. Interface Focus. 2015; 5(5):13.
37. Atchley AA, Prosperetti A. The crevice model of bubble nucleation. J. Acoust. Soc. Am. 1989; 86(3):1065–1084.
38. Jones SF, Evans GM, Galvin KP. Bubble nucleation from gas cavities - a review. Adv. Colloid Interface Sci. 1999; 80(1):27–50.
39. Miller DL. Experimental investigation of the response of gas-filled micropores to ultrasound. J. Acoust. Soc. Am. 1982; 71(2):471–476.
40. Seddon JRT, Kooij ES, Poelsema B, Zandvliet HJW, Lohse D. Surface Bubble Nucleation Stability. Phys. Rev. Lett. 2011; 106(5):056101. [PubMed: 21405411]

41. Borkent BM, Gekle S, Prosperetti A, Lohse D. Nucleation threshold and deactivation mechanisms of nanoscopic cavitation nuclei. Phys. Fluids. 2009; 21(10):102003.
42. Belova V, Shchukin DG, Gorin DA, Kopyshev A, Mohwald H. A new approach to nucleation of cavitation bubbles at chemically modified surfaces. Phys. Chem. Chem. Phys. 2011; 13(17):8015–8023. [PubMed: 21448506]
43. Yildirim A, Demirel GB, Erdem R, Senturk B, Tekinay T, Bayindir M. Pluronic polymer capped biocompatible mesoporous silica nanocarriers. Chem. Comm. 2013; 49(84):9782–9784. [PubMed: 24026175]
44. Bouchoucha M, C-Gaudreault R, Fortin MA, Kleitz F. Mesoporous Silica Nanoparticles: Selective Surface Functionalization for Optimal Relaxometric and Drug Loading Performances. Adv. Func. Mater. 2014; 24(37):5911–5923.
45. He QJ, Cui XZ, Cui FM, Guo LM, Shi JL. Size-controlled synthesis of monodispersed mesoporous silica nano-spheres under a neutral condition. Micropor. Mesopor. Mater. 2009; 117(3):609–616.
46. Shen D, Yang J, Li X, Zhou L, Zhang R, Li W, Chen L, Wang R, Zhang F, Zhao D. Biphase Stratification Approach to Three-Dimensional Dendritic Biodegradable Mesoporous Silica Nanospheres. Nano Lett. 2014; 14(2):923–932. [PubMed: 24467566]
47. Stober W, Fink A, Bohn E. Controlled growth of monodisperse silica spheres in micron size range. J. Colloid Interface Sci. 1968; 26(1):62–69.
48. Yasui, K., Tuziuti, T., Kanematsu, W., Kato, K. Langmuir. ASAP; 2016.
49. Chattaraj R, Mohan P, Besmer JD, Goodwin AP. Selective Vaporization of Superheated Nanodroplets for Rapid, Sensitive, Acoustic Biosensing. Adv. Healthcare Mater. 2015; 4(12): 1790–1795.
50. Kim JM, Chang SM, Kong SM, Kim KS, Kim J, Kim WS. Control of hydroxyl group content in silica particle synthesized by the sol-precipitation process. Ceram. Int. 2009; 35(3):1015–1019.
51. Primeau N, Vautey C, Langlet M. The effect of thermal annealing on aerosol-gel deposited SiO2 films: a FTIR deconvolution study. Thin Solid Films. 1997; 310(1–2):47–56.
52. Zhang TR, Ge JP, Hu YX, Zhang Q, Aloni S, Yin YD. Formation of hollow silica colloids through a spontaneous dissolution-regrowth process. Angew. Chem. Int. Ed. 2008; 47(31):5806–5811.
53. Zhu H, Ma YG, Fan YG, Shen JC. Fourier transform infrared spectroscopy and oxygen luminescence probing combined study of modified sol-gel derived film. Thin Solid Films. 2001; 397(1–2):95–101.
54. Zhuravlev LT. The surface chemistry of amorphous silica. Zhuravlev model. Colloids Surf. A. 2000; 173(1–3):1–38.
55. Comas-Vives A. Amorphous SiO2 surface models: energetics of the dehydroxylation process, strain, ab initio atomistic thermodynamics and IR spectroscopic signatures. Phys. Chem. Chem. Phys. 2016; 18(10):7475–7482. [PubMed: 26898649]
56. Binks BP, Lumsdon SO. Influence of particle wettability on the type and stability of surfactant-free emulsions. Langmuir. 2000; 16(23):8622–8631.
57. Lundqvist M, Stigler J, Cedervall T, Berggard T, Flanagan MB, Lynch I, Elia G, Dawson K. The Evolution of the Protein Corona around Nanoparticles: A Test Study. ACS Nano. 2011; 5(9):7503–7509. [PubMed: 21861491]
58. Tenzer S, Docter D, Kuharev J, Musyanovych A, Fetz V, Hecht R, Schlenk F, Fischer D, Kiouptsi K, Reinhardt C, Landfester K, Schild H, Maskos M, Knauer SK, Stauber RH. Rapid formation of plasma protein corona critically affects nanoparticle pathophysiology. Nat. Nanotechnol. 2013; 8(10):772–781. [PubMed: 24056901]
59. Binks BP, Horozov TS. Aqueous foams stabilized solely by silica nanoparticles. Angew. Chem. Int. Ed. 2005; 44(24):3722–3725.
60. Zhang HY, Dunphy DR, Jiang XM, Meng H, Sun BB, Tarn D, Xue M, Wang X, Lin SJ, Ji ZX, Li RB, Garcia FL, Yang J, Kirk ML, Xia T, Zink JI, Nel A, Brinker CJ. Processing Pathway Dependence of Amorphous Silica Nanoparticle Toxicity: Colloidal vs Pyrolytic. J. Amer. Chem. Soc. 2012; 134(38):15790–15804. [PubMed: 22924492]
61. Hobbs SK, Monsky WL, Yuan F, Roberts WG, Griffith L, Torchilin VP, Jain RK. Regulation of transport pathways in tumor vessels: Role of tumor type and microenvironment. Proc. Natl. Acad. Sci. USA. 1998; 95(8):4607–4612. [PubMed: 9539785]

62. Cassie ABD, Baxter S. Large contact angles of plant and animal surfaces. Nature. 1945; 155(3923):21–22.

63. Marschall HB, Morch KA, Keller AP, Kjeldsen M. Cavitation inception by almost spherical solid particles in water. Phys. Fluids. 2003; 15(2):545–553.

64. Morch KA. Reflections on cavitation nuclei in water. Phys. Fluids. 2007; 19(7):072104.

65. Arora M, Ohl CD, Morch KA. Cavitation inception on microparticles: A self-propelled particle accelerator. Phys. Rev. Lett. 2004; 92(17):174501. [PubMed: 15169155]

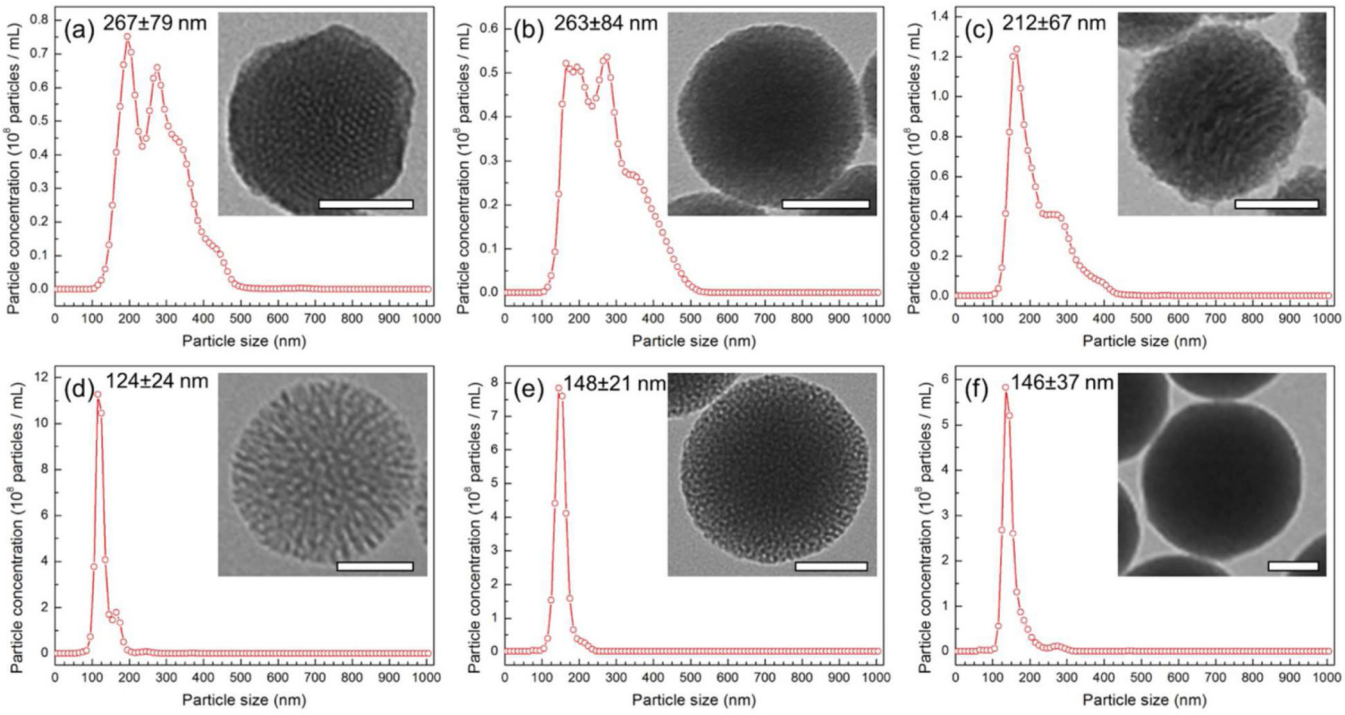

Figure 1.

Size distributions of the silica nanoparticles in water as determined by Nanoparticle Tracking Analysis; a) MCM-41, b) MCM-48S, c)MCM-48R, d) Dendritic, e) Random, and f) Solid. Insets show the TEM images of the silica nanoparticles. Scale bars are 50 nm.

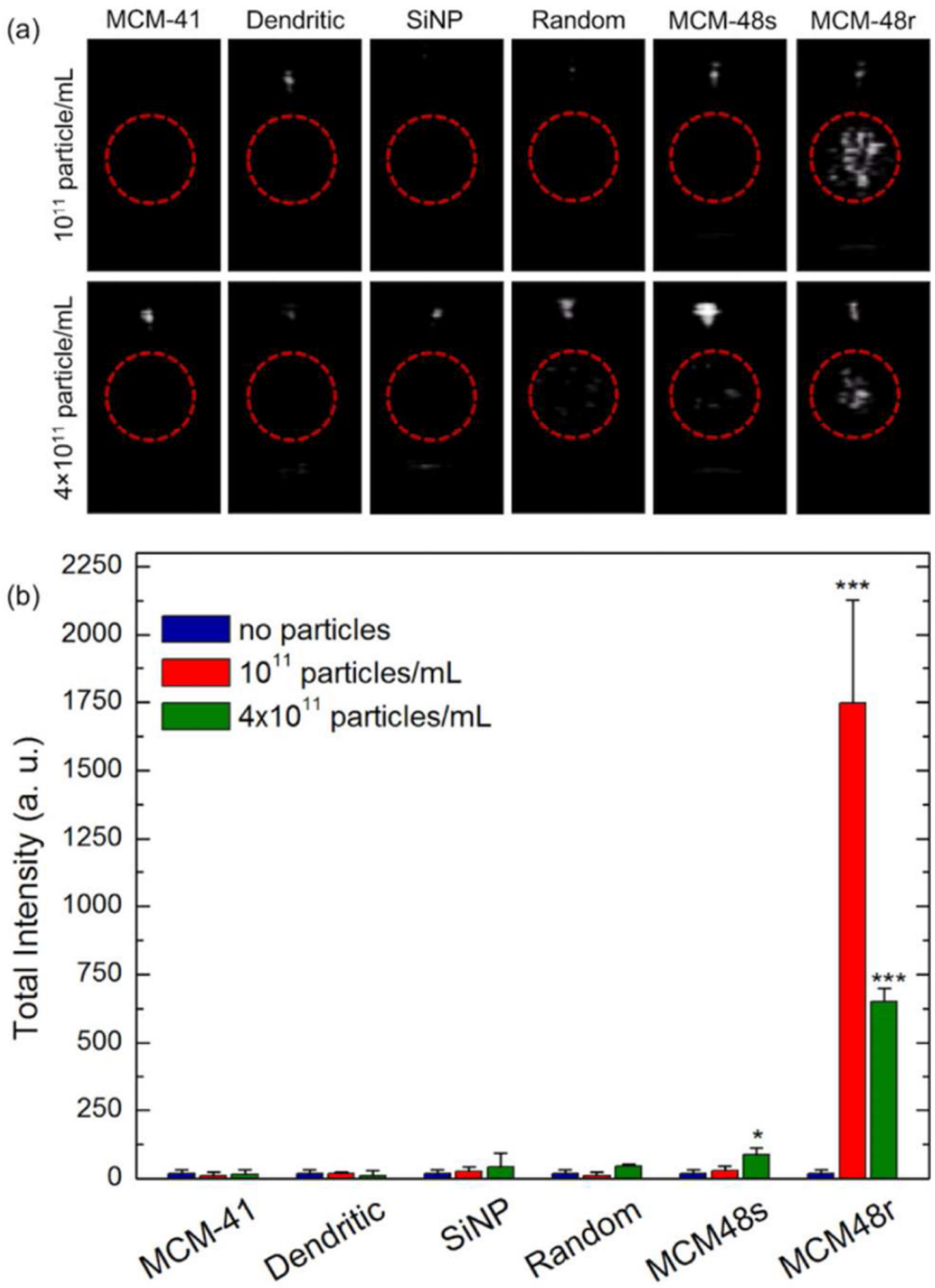

Figure 2.

(a) Representative images taken from movies acquired during HIFU insonation of nanoparticles at two different concentrations. Red circles mark the region of interest (ROI), or the area shows the focus of the HIFU. The white spot above the ROI is due to reflection from the sample tube wall. (b) Calculated total intensities from the acquired movies of the samples at two different particle concentrations. Error bars = 1 SD, studies were run in triplicate. Student's t test was applied to the data; * indicates $p<0.05$ and *** indicates $p<0.0001$.

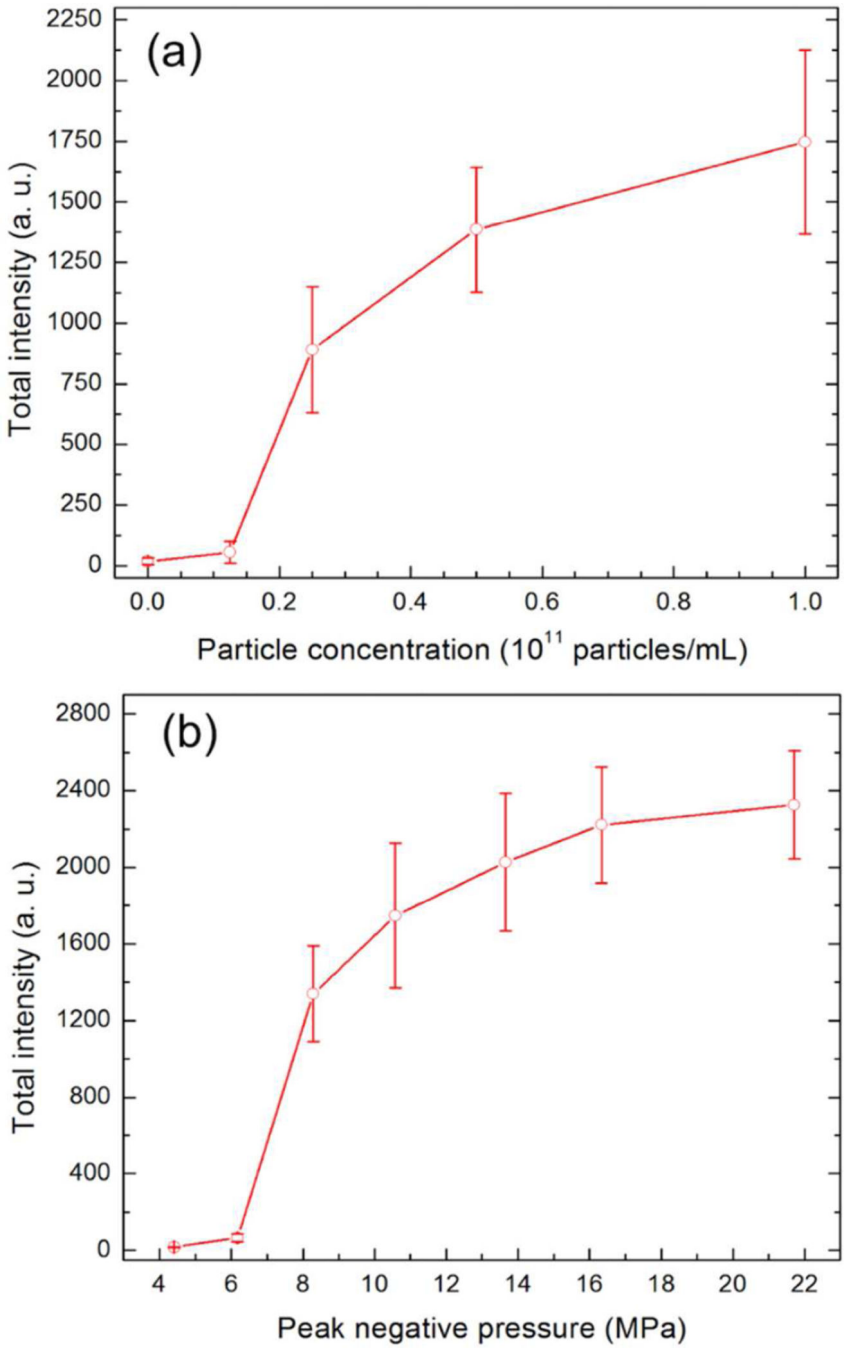

Figure 3.

(a) Effect of the particle concentration on the total intensity generated by MCM-48R at peak negative pressure of 10.6 MPa. (b) Effect of peak negative pressure on the total intensity generated by MCM-48R at the particle concentration of 10^{11} particles mL^{-1}. Error bars = 1 SD, studies were run in triplicate.

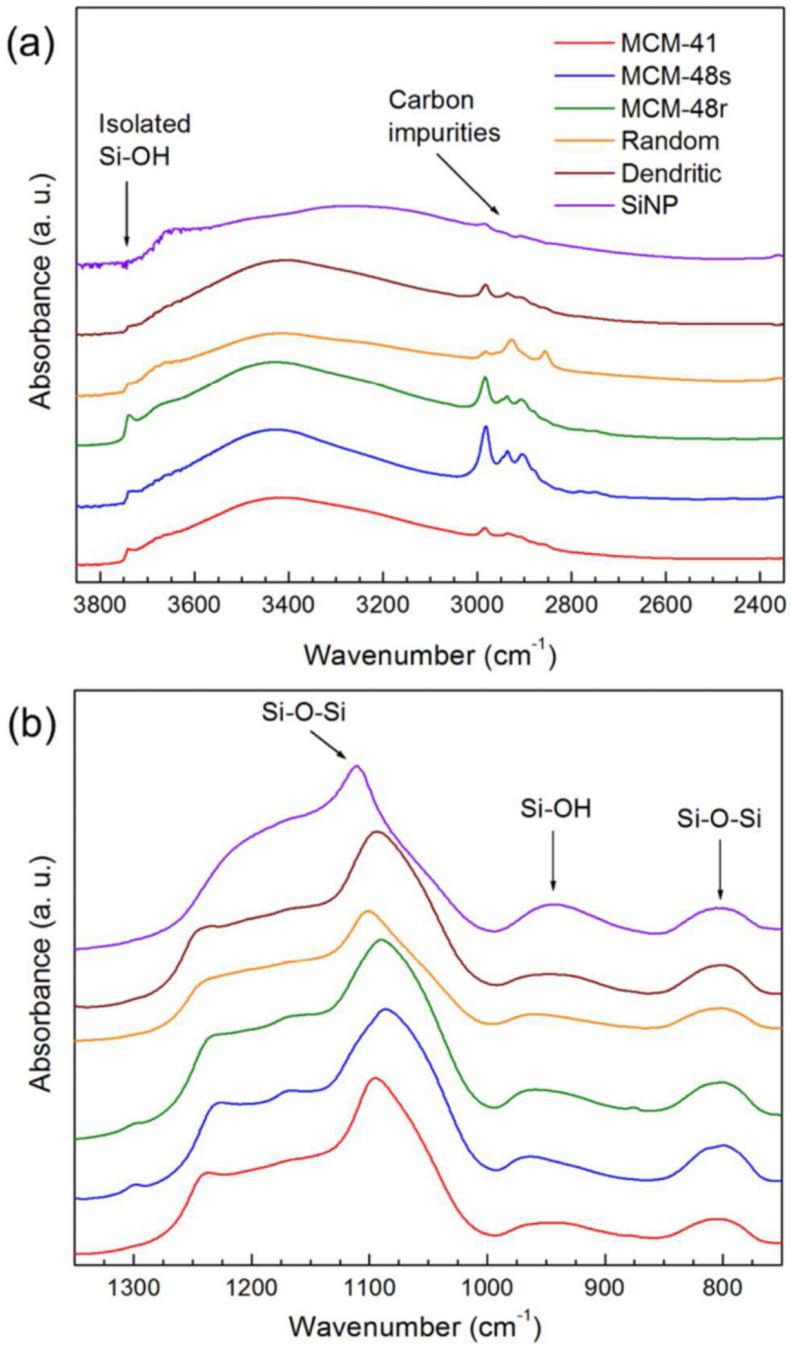

Figure 4.

FTIR spectra of the silica nanoparticles. (a) The range of FTIR spectra (3850-2450 cm^{-1}) showing the isolated and interacting hydroxyl and carbon impurity absorption bands of the nanoparticles. (b) The range of FTIR spectra (1400-700 cm^{-1}) showing the silanol and siloxane absorption bands of the nanoparticles.

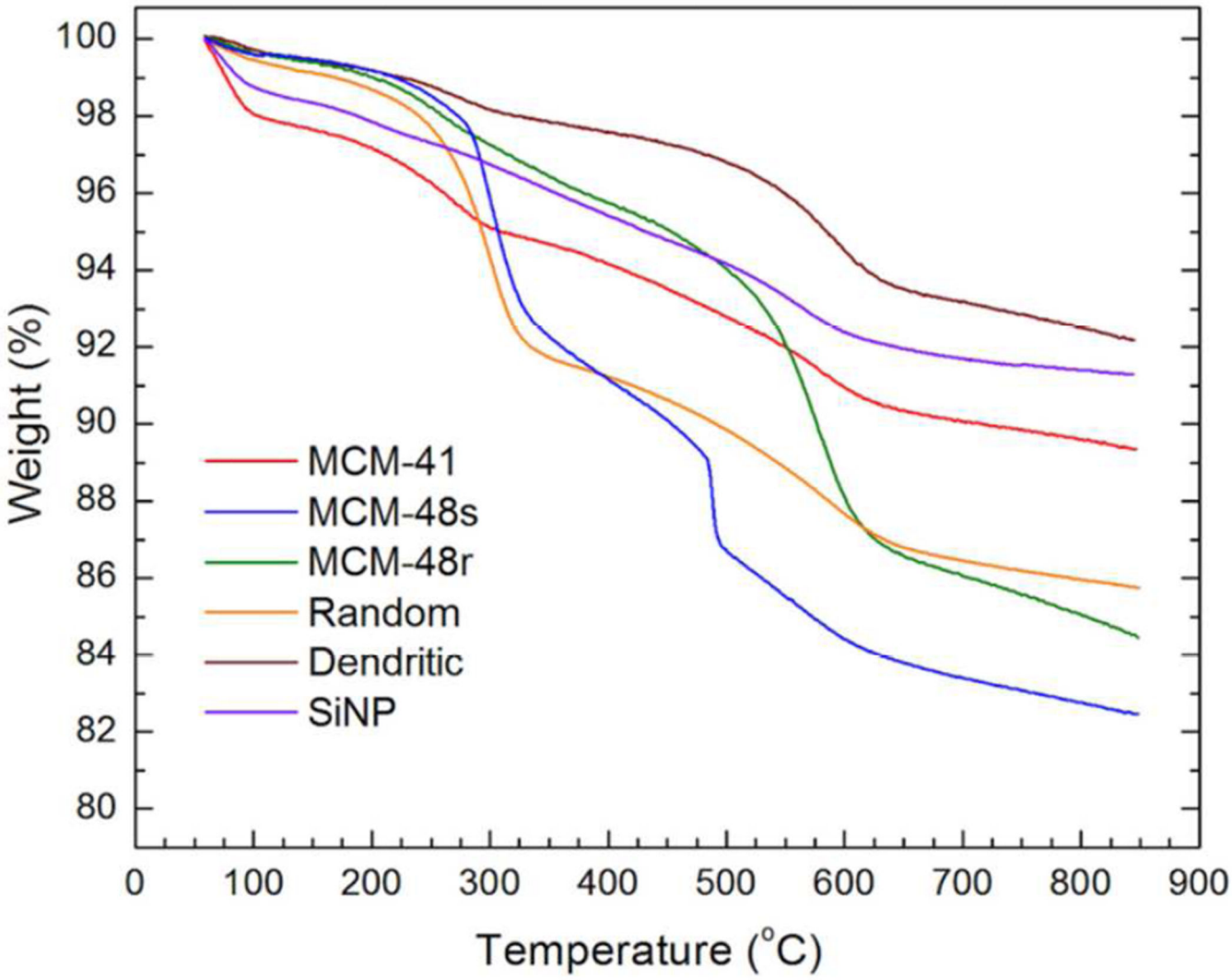

Figure 5.
TGA curves of the silica nanoparticles.

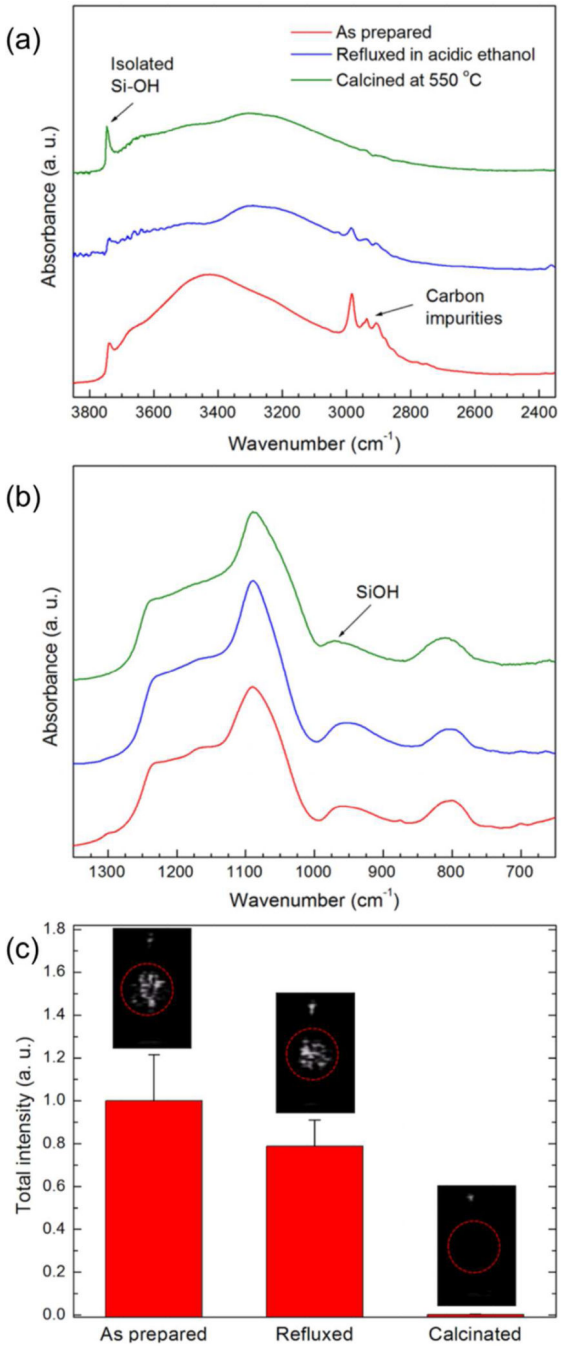

Figure 6.

FTIR spectra of the as-prepared, refluxed in acidic ethanol, and calcined MCM-48R. (a) The range of FTIR spectra (3850-2450 cm^{-1}) showing the isolated and interacting hydroxyl and carbon impurity absorption bands of the nanoparticles. (b) The range of FTIR spectra (1400-700 cm^{-1}) showing the hydroxyl and siloxane absorption bands of the nanoparticles. (c) Calculated total intensities from the acquired movies of the as prepared, refluxed in ethanol, and calcinated MCM-48R samples at a particle concentration of 10^{11} particles mL^{-1}. Insets are the representative images taken from movies acquired during HIFU

insonation. Red circles mark the region of interest. Error bars = 1 SD, studies were run in triplicate.

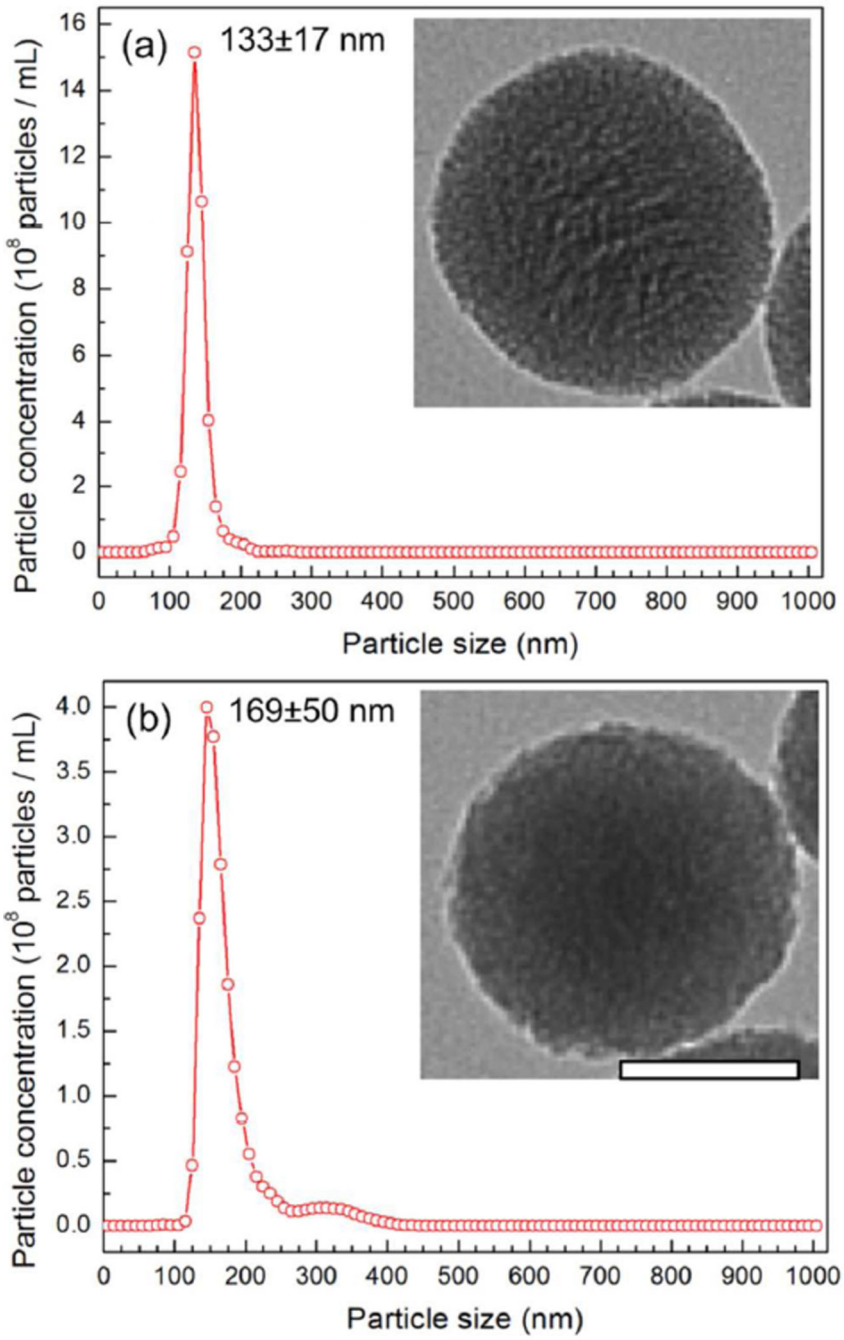

Figure 7.

Size distributions of the (a) MCM-48D and (b) MCM-48MD in water as determined by Nanoparticle Tracking Analysis. Insets show the TEM images of the silica nanoparticles. Scale bars are 50 nm.

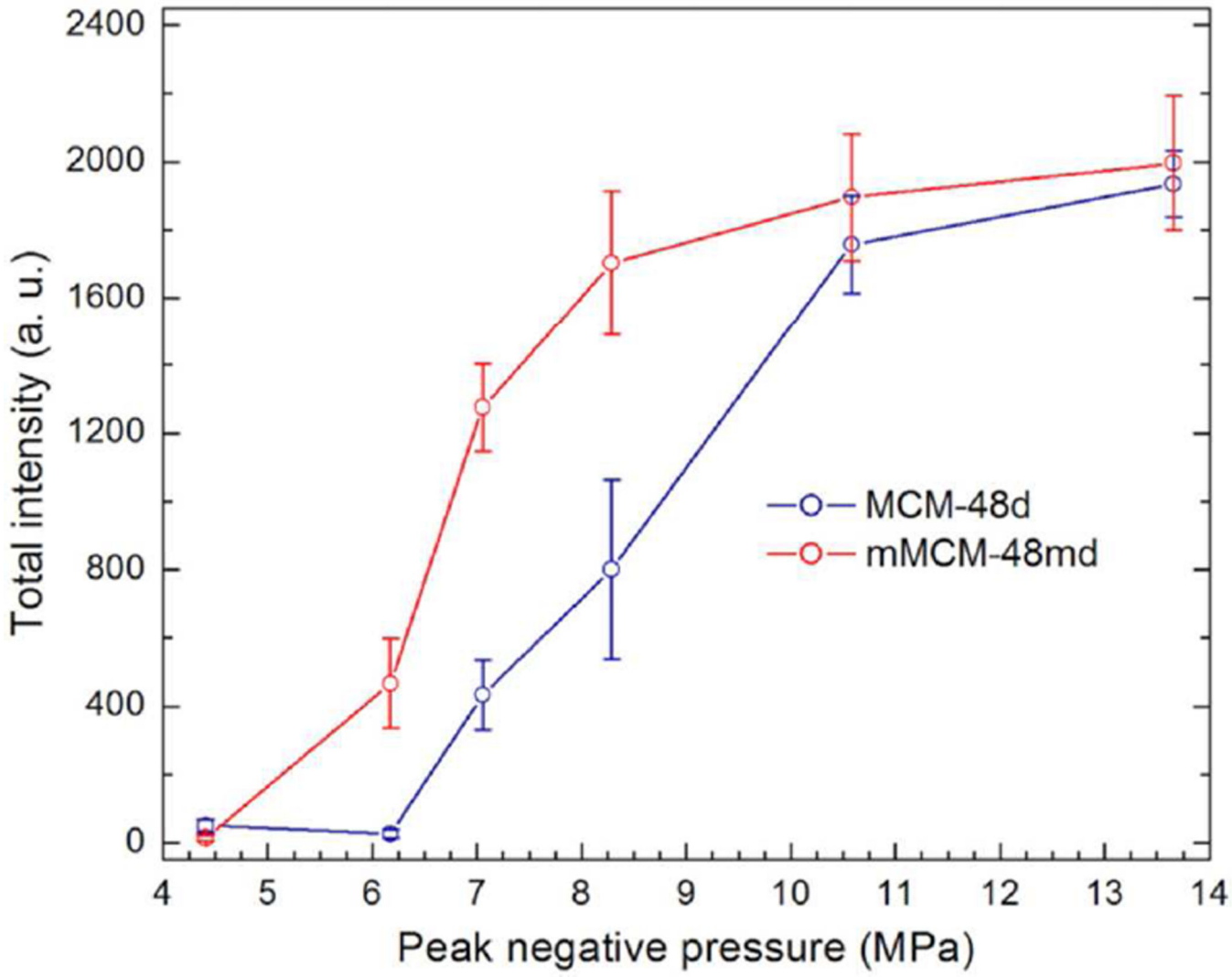

Figure 8.

Effect of peak negative pressure on the total intensity generated by MCM-48D and MCM-48MD at the particle concentration of 10^{11} particles mL^{-1}. Error bars = 1 SD, studies were run in triplicate.

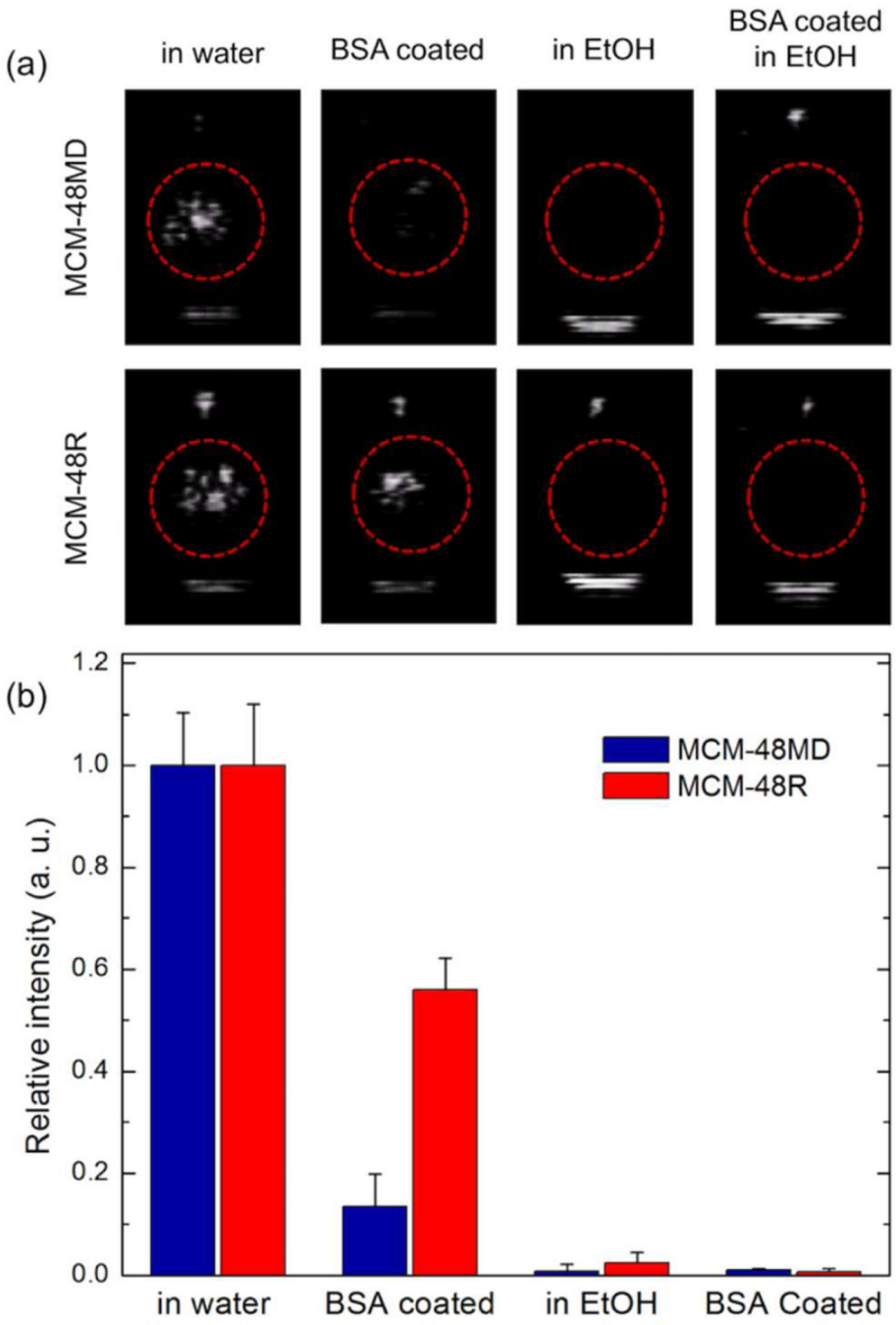

Figure 9.

(a) Representative images taken from movies acquired during HIFU insonation of nanoparticles with or without BSA coating in 90% ethanol or water. Red circles mark the region of interest. (b) Calculated total intensities from the acquired movies of nanoparticles with or without BSA coating in water and in 90% ethanol at a particle concentration of 10^{11} particles mL^{-1}. Error bars = 1 SD, studies were run in triplicate.

Table 1

Particle sizes and concentrations of the silica nanoparticles as determined by TEM and NTA.

	TEM Size (nm)	NTA Size (nm)	Particle number (in 1 mg mL^{-1})[a]
MCM-41	112±18	267±79	$0.32\times^{10}$
MCM-48S	92±15	263±84	0.56×10^{12}
MCM-48R	94±10	212±67	0.63×10^{12}
Dendritic	111±7	124±24	1.89×10^{12}
Random	137±10	148±21	1.48×10^{12}
Solid	121±12	146±37	1.09×10^{12}

[a]Determined by NTA.

Table 2

Threshold pressures for acoustic cavitation of water in the presence of silica nanoparticles.

	Particle concentration (10^{11} particles mL^{-1})		Particle concentration (4×10^{11} particles mL^{-1})	
	Threshold (MPa)	**Description**	**Threshold (MPa)**	**Description**
MCM-41	>22	No response	>22	No response
MCM-48S	>22	No response	9.1	Weak response
MCM-48R	6.2	Strong response	6.2	Strong response
Dendritic	>22	No response	>22	No response
Random	>22	No response	6.2	Response dies off quickly
Solid	>22	No response	>22	No response